

Behaviour and Modelling of Dual-Phase Steels

Venkatapathi Tarigopula, Odd Sture Hopperstad, Magnus Langseth and Arild Holm Clausen

Structural Impact Laboratory (SIMLab), Centre for Research-based Innovation and Department of Structural Engineering, Norwegian University of Science and Technology (NTNU)

Richard Brikelandsvei 1A, NO-7491 Trondheim, Norway

Summary:

Dual-phase steels are being increasingly considered for application in vehicle structural crash components because of their combined attributes of high-strength and good formability characteristics. Accurate prediction of such components, which are often made of formed components, is necessary to reduce the cost of physical tests. The non-linear finite element method is an efficient and reliable tool for the design of new components. The reliability of the finite element analyses depends on the accuracy of the constitutive and fracture models. To support the engineering applications of dual-phase steels for crash and forming events, both strain hardening and strain rate hardening must be thoroughly modelled for general loading paths.

In this paper, an elasto-viscoplastic phenomenological model is adopted to represent the material behaviour of dual-phase steels. The constitutive model is formulated in the framework of phenomenological continuum mechanics. The main ingredients of the model include a non-quadratic yield criterion, the associated flow rule and non-linear isotropic and kinematic hardening. The model is within the class of plasticity models proposed by Chaboche [1] and Lemaitre and Chaboche [2] for application to monotonic, non-proportional and cyclic loading conditions. The constitutive model is also able to depict viscous characteristics of the material.

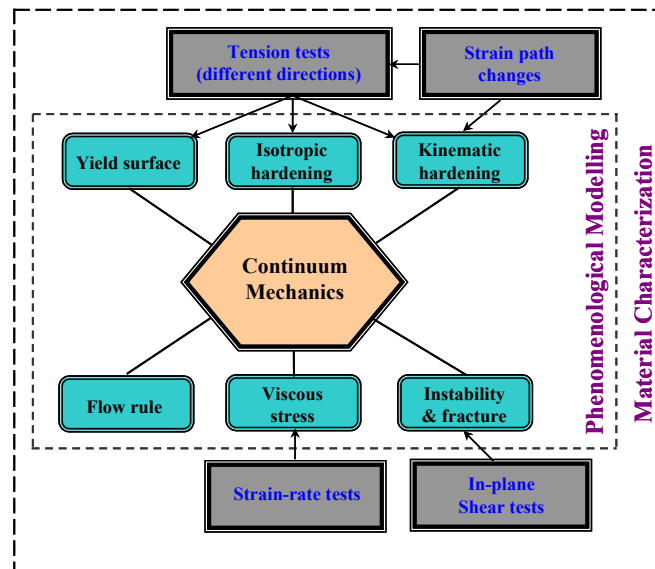


Figure 1. Identification of material parameters for the chosen constitutive model

The material was experimentally characterized under different loading conditions suited for crash and forming events. Figure 1 depicts the approach embraced in this research for identification of material parameters for the utilized model from material tests. The conventional material tests are providing data for the calibration of the model. Simple tension tests were used to characterize the elastic parameters, the yield surface and the isotropic hardening parameters. Non-proportional tension tests were used to identify the kinematic hardening parameters. Additionally, viscous parameters were identified from the corresponding tension tests over a wide range of strain-rates.

The predictive capability of the adopted numerical model is assessed against the material behaviour at elevated rates of strain and the material behaviour under strain-path changes. Particularly, phenomena like dynamic localisation, large plastic deformations have given due importance for validity of the numerical model. Moreover, the same model is validated for crashworthiness performance of dual-phase steel generic components. The model provides results which are in good agreement with the experimental observations. In this work, the non-linear explicit FE code LS-DYNA was used for numerical computations.

Keywords:

Dual-phase steels, Numerical simulations, Material modelling, LS-DYNA, Non-proportional loading and Crashworthiness.

1 Introduction

Thin-walled steel sections are of the most important components in an automotive body because of their large ability with respect to weight to absorb energy in the case of a crash event, and thereby ensuring the integrity of the passenger compartment. Thus, the automotive industry has certainly pushed the research within this field during the last years due to an increased focus on safety and weight savings. Besides, the steel industry itself has been eager to improve the knowledge and performance of steel sections in order to maximize the utilization of steel and maintain its competitiveness with alternative materials such as aluminium, composites and plastics. In response to the automotive industry's demand to reduce overall vehicle weight and thereby improve fuel economy, and to satisfy safety and crashworthiness requirements, the steel industry has developed a large variety of steels with increased energy absorbing properties allowing down gauging of body-in-white components. Especially dual-phase high-strength steels that exhibit high strength and enhanced formability hogged the lime light. Compared to conventional steels, relatively little knowledge have been gained for high-strength steel structures subjected to impact loading conditions. Therefore, this paper is intended to provide more insight on the behaviour and modelling of dual-phase high-strength steels with respect to crash and forming applications.

The reliability of finite element analyses depends on the accuracy of constitutive and fracture models. A suitable material model for dual-phase steels called the Weak Texture Model (WTM) has previously been implemented in LS-DYNA [3]. The main objective of this work is to evaluate the performance of the constitutive model for various deformation modes of dual-phase steel subjected to general loading paths. The parameters in constitutive model are identified from various material characterization tests, both traditional ones as uniaxial tensile tests and others more specifically to identify certain model parameters.

At first the material model is presented, followed by the results from the material tests and the corresponding identification of material parameters. Finally, the constitutive model is validated for crashworthiness of dual-phase steel generic components.

2 Material characterization tests

In the present study, cold reduced dual-phase high-strength steel DP800 was investigated. This steel is subjected to special heat treatment in the continuous annealing line, which produces a two phase structure, namely ferrite that imparts unique forming properties, and martensite that explicates the strength. All specimens in this study were taken from a sheet with thickness of 1.5 mm and the corresponding variation along the sheet was less than 2 %.

Material tests were carried out to characterize the materials and on this basis identify material parameters. Standard quasi-static uniaxial tensile tests were carried out in three directions to study anisotropy, and calibrate the strain hardening parameters. Furthermore, dynamic tensile tests were performed to account for strain-rate sensitivity, and the results were used to include possible strain-rate effects in the material models.

2.1 Quasi-static tensile tests

The stress-strain behaviour of the materials was obtained from standard quasi-static tensile tests. All tests were carried out with a specimen of gauge length 30 mm and 5 mm in width, as depicted in Figure 2, at a strain rate of approximately 10^{-3} s^{-1} . Tensile specimens were extracted along the rolling direction, 45° to the rolling direction, and in the transverse in-plane direction from the as-received sheet. Three repetitions in each direction were used to examine the scatter in the results. For each test the applied load and the crosshead displacement were recorded digitally with data acquisition software at a frequency of 10 Hz. In addition, the strains in the length direction were determined continuously by a one-sided longitudinal extensometer with 20 mm gauge length, while width strains were found by employing a transverse average extensometer. Standard equations were utilized to determine the nominal and true stress-strain curves from the measured force-deformation curves.

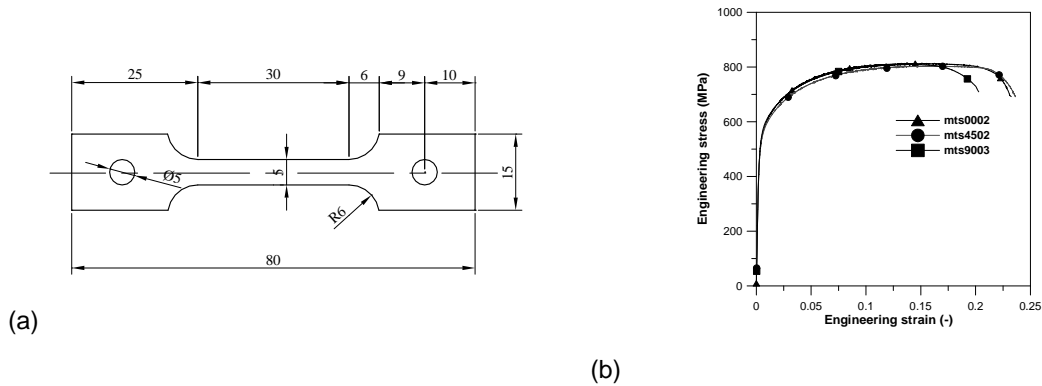


Figure 2. (a) Specimen geometry for quasi-static tensile tests, and (b) Engineering stress-strain curves.

Typical engineering stress-strain curves from the tensile tests are shown in Figure 2b. The scatter in the repetitive tests is small, thus it is allowable to select a representative test to illustrate the experimental trends. One representative test is chosen to represent the behaviour. As can be seen from Figure 2b that the yield strength of the material is wavering around 520 MPa and the ultimate strength is approximately 800 MPa. It is also revealed that very little scatter in material properties in three different orientations, which means that the anisotropy in the material is negligible.

2.2 Dynamic tensile tests

The dynamic stress-strain behaviour of DP800 was acquired from dynamic tensile tests, carried out over a wide range of nominal strain rates in order to investigate the strain rate sensitivity. Dynamic tensile tests were carried out at room temperature at a strain rate in the range of 10^{-3} to 600 s^{-1} . Low strain rate tests (10^{-3} - 10^0 s^{-1}) were carried out in conventional servo-hydraulic machine, while high strain-rate tests (150 - 600 s^{-1}) were performed on split-Hopkinson tension bar (SHTB) [4]. In SHTB as illustrated in Figure 3, the specimen was sandwiched between the two long bars of diameter 10 mm. The incident, reflected and transmitted pulses were recorded with strain gauges mounted at positions ② and ③ on the incident and out-put bar. The transmitted part of the wave accounts for a measure of the load on the specimen, while the reflected part gives a measure of the specimen deformation. Further details regarding the set-up and results processing are provided by Clausen and Auestad [4].

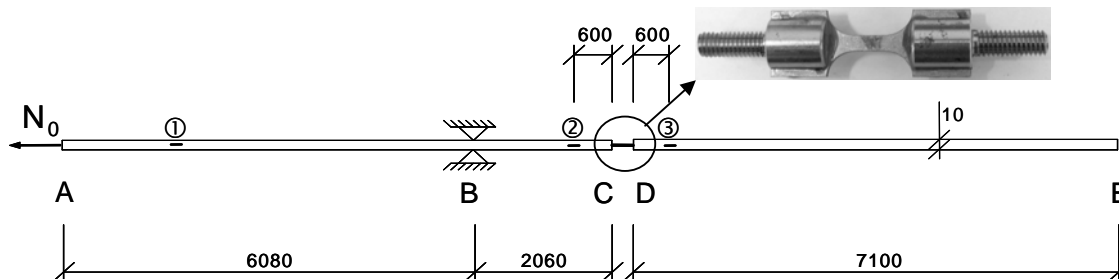


Figure 3. A schematic diagram of SHTB at SIMLab, NTNU along with sheet specimen.

The true stress-strain curves until diffuse necking are given in Figure 4. As one can see, there is significant influence of the strain rate with respect to strength and the increase of dynamic flow stress is approximately 12 % within the investigated strain-rate range.

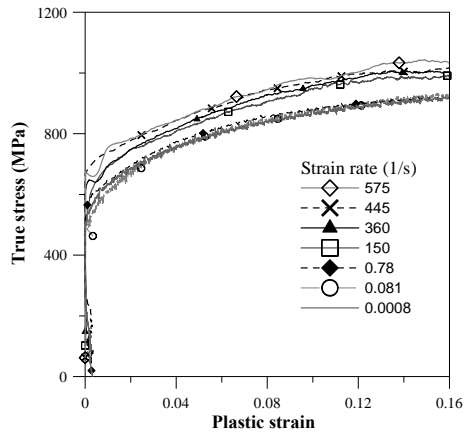


Figure 4. True stress-plastic strain curves from dynamic tensile tests.

2.3 Shear tests

Shear tests were carried out in three different orientations. A shear test specimen [5, 6] designed for determining the plastic behaviour of sheet metals at large deformations was adopted for testing in the current study and the corresponding specimen geometry is shown in Figure 5a. The specimen is developed in such a way that it can be mounted and tested in a standard tensile testing machine. It should be mentioned that shear test allows for effective plastic strains up to 1 in the shear zone with minimal or no presence of plastic instabilities before failure, i.e. several magnitudes higher than the strain obtained before onset of diffuse necking in a uniaxial tensile test. A detailed description of the specimen is found in Tarigopula et al. [7]. The specimens were mounted with the longitudinal direction in the tension direction in a Dartec 20 kN testing machine, and then the tests were carried out under displacement control at a displacement rate of approximately 0.3 mm/min, producing an average strain rate of about $2 \cdot 10^{-3} \text{ s}^{-1}$. The displacement in the length direction was measured by an Instron one-sided extensometer with 20 mm gauge length.

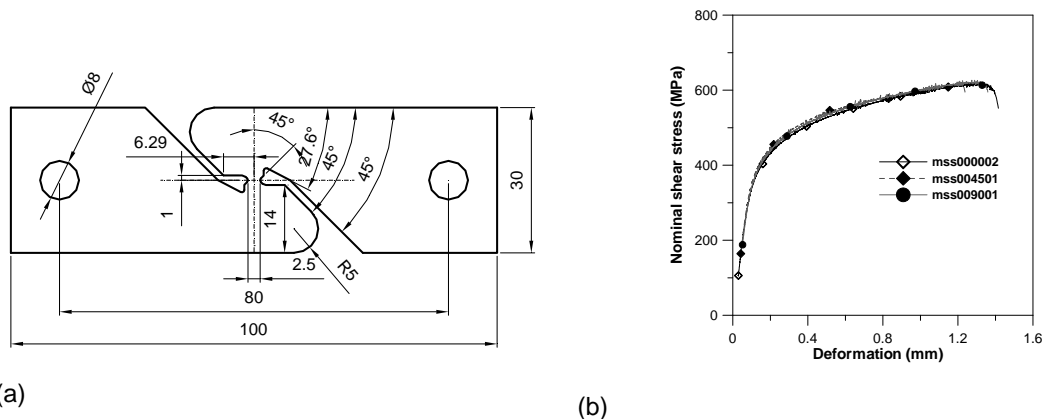


Figure 5. (a) Geometry of the shear specimen, and (b) Nominal shear stress-deformation curves from the shear tests

The test results in terms of nominal shear stress-elongation characteristics are presented in Figure 5b. The nominal shear stress is the applied force divided by the nominal cross-sectional area of the shear zone. Only minor variation between two duplicate tests was found, and thereby one test was chosen to represent the behaviour. The increase of the nominal shear stress is gradual, and the curves do not exhibit any drop in flow stress. Furthermore, the nominal shear stress-elongation curves show minor signs of plastic instability taking place before the onset of failure occurs at maximum force. It is noteworthy that the differences in the calculated nominal shear stress-deformation curves between various directions, as displayed in Figure 5b, are very small for the virgin material.

2.4 Tensile tests after pre-straining

The elastic-plastic behaviour of dual-phase, high-strength steel sheets under two-stage strain-path changes has been investigated. Uniaxial tension tests in different directions are carried out after pre-strained in uniaxial tension. Dual-phase DP800 steel sheet of 1.5 mm was pre-strained in uniaxial tension to effective strains of about 1 %, 4 % and 8 %. Pre-straining was performed in the rolling direction by pulling large tensile specimens at a cross-head speed of 2 mm/min using a Dartec 500 kN hydraulic testing machine and then unloading at the same rate. The gauge section of these large specimens was approximately 102 mm wide and 500 mm long. The amount of deformation during pre-straining was determined by measuring the sample elongation over the gauge length.

Thereafter, sub-size tension specimens, as shown in Figure 2a, were machined from the pre-strained large tensile samples at various angles to the pre-strain axis in order to subject them to a second deformation path. Tensile tests after pre-straining were carried out with the same procedure as described in Section 3.1. Typical true stress-strain curves of the pre-deformed DP800 are presented in Figure 6. One representative test is chosen from the three repetitions for each direction to show the behaviour. As seen from Figure 6, the initial flow stress (or yield stress) is strongly dependent on the orientation of reloading after pre-straining. For all pre-strains, the reloading in different strain paths produced transient hardening behaviour that is characterized by rounding of the flow curve, yielding at low stresses and rapid change of work hardening rate. This behaviour gives an indication of the presence of kinematic hardening in the material at the early stage. It is also interesting to observe that after a transient stage, the difference in flow stress diminishes as tensile deformation progresses regardless of the orientation

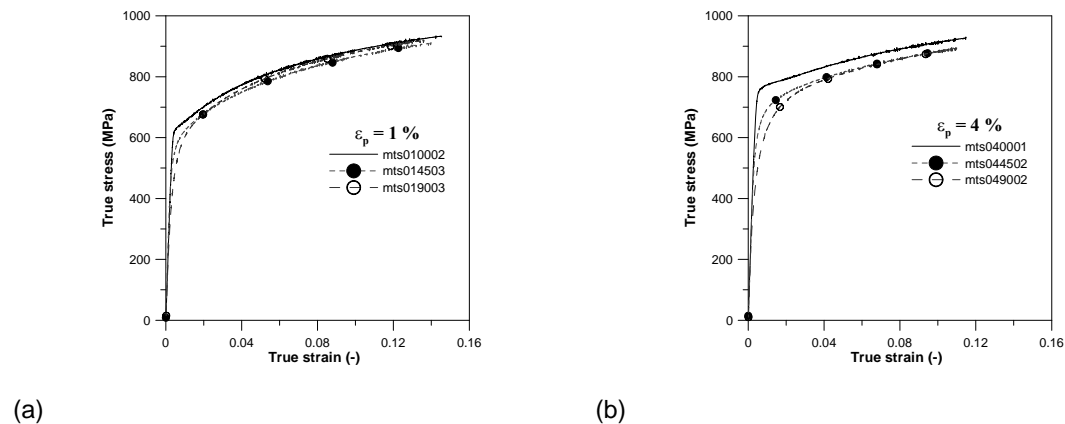


Figure 6. Tensile stress-strain curves for one representative test from each direction for (a) 1 % pre-strained sheet and (b) 4 % pre-strained sheet.

3 Material modelling

The weak texture model (*MAT_135) that has been implemented in LS-DYNA [3] was used in the present study. The constitutive model is formulated in the framework of phenomenological continuum mechanics. The main ingredients of the model include a non-quadratic yield criterion, the associated flow rule and non-linear isotropic and kinematic hardening. The model is within the class of plasticity models proposed by Chaboche [1] and Lemaitre and Chaboche [2] for application to monotonic, non-proportional and cyclic loading conditions. The basic equations of the model are collected in Table 1. The small-strain formulation is presented in the table, while large rotations are accounted for by use of a co-rotational formulation [8]. Based on the initial isotropy of the as-received material, an isotropic yield function is selected. The model adopts a convex, high-exponent, isotropic yield function that includes the von Mises yield criterion as a special case ($m = 2$). In the present study, $m = 6$ was used. The viscous characteristics of the material are defined by modified Johnson-cook model [9].

Additive decomposition of strain rate tensor into elastic and plastic parts:

$$\dot{\boldsymbol{\varepsilon}} = \dot{\boldsymbol{\varepsilon}}^e + \dot{\boldsymbol{\varepsilon}}^p$$

Elastic stress-strain relation on rate form:

$$\dot{\boldsymbol{\sigma}} = \mathbf{E} : \dot{\boldsymbol{\varepsilon}}^e = \mathbf{E} : (\dot{\boldsymbol{\varepsilon}} - \dot{\boldsymbol{\varepsilon}}^p)$$

Yield surface:

$$f(\boldsymbol{\Sigma}, R) = \bar{\sigma}(\boldsymbol{\Sigma}) - (Y_0 + R) = 0$$

Equivalent stress:

$$\bar{\sigma}(\boldsymbol{\Sigma}) = \left\{ \frac{1}{2} \left[|\Sigma_1 - \Sigma_2|^m + |\Sigma_2 - \Sigma_3|^m + |\Sigma_3 - \Sigma_1|^m \right] \right\}^{\frac{1}{m}}$$

Associated flow rule - rate independent:

$$\dot{\boldsymbol{\varepsilon}}^p = \dot{\lambda} \frac{\partial f}{\partial \boldsymbol{\Sigma}}; \quad \dot{R} = -\dot{\lambda} \frac{\partial f}{\partial R} = \dot{\lambda}$$

Non-linear isotropic hardening rule:

$$\dot{R} = \sum_{i=1}^2 \dot{R}_i = \sum_{i=1}^2 C_{Ri} (Q_{Ri} - R_i) \dot{\lambda}$$

Non-linear kinematic hardening rule:

$$\dot{\mathbf{X}} = \sum_{i=1}^2 \dot{\mathbf{X}}_i = \sum_{i=1}^2 C_{Xi} (Q_{Xi} \frac{\boldsymbol{\Sigma}}{\bar{\sigma}(\boldsymbol{\Sigma})} - \mathbf{X}_i) \dot{\lambda}$$

Loading/unloading conditions in Kuhn-Tucker form:

$$f \leq 0; \quad \dot{\lambda} \geq 0; \quad \dot{\lambda} f = 0,$$

Overstress tensor:

$$\boldsymbol{\Sigma} = \boldsymbol{\sigma} - \mathbf{X} = \boldsymbol{\sigma} - \sum_{i=1}^2 \mathbf{X}_i$$

Plastic flow rate- rate dependent:

$$\dot{\lambda} = \frac{\phi(f)}{\eta}$$

Table 1. Basic constitutive equations (small strain formulation)

4 Identification of material parameters

The results from the material tests are used in the following to determine the parameters in the constitutive model for the dual-phase steel.

4.1 Strain hardening and strain-rate hardening

The representation of the equivalent stress vs. equivalent strain curve in uniaxial tension as

$$\bar{\sigma} = \left(\sigma_0 + \sum_{i=1}^2 Q_i (1 - \exp(-C_i \bar{\varepsilon})) \right) \left(1 + \frac{\dot{\bar{\varepsilon}}}{\dot{\varepsilon}_0} \right)^q, \quad (1)$$

where σ_0 , Q_i , C_i and q are material constants, $\bar{\varepsilon}$ is the effective plastic strain, $\dot{\bar{\varepsilon}}$ is the effective plastic strain-rate and $\dot{\varepsilon}_0$ is a user-defined reference strain-rate. The first factor in the equation

governs strain hardening, while second factor defines the rate dependent behaviour (viscoplasticity). The basic strain hardening parameters σ_0 , Q_i and C_i ($i = 1, 2$) were found by curve fitting the equation, Eq. (1), to the true stress-strain curves in the 0° direction, which is chosen as the reference direction. Figure 7a shows that this selected model describes the experimental behaviour very well before necking.

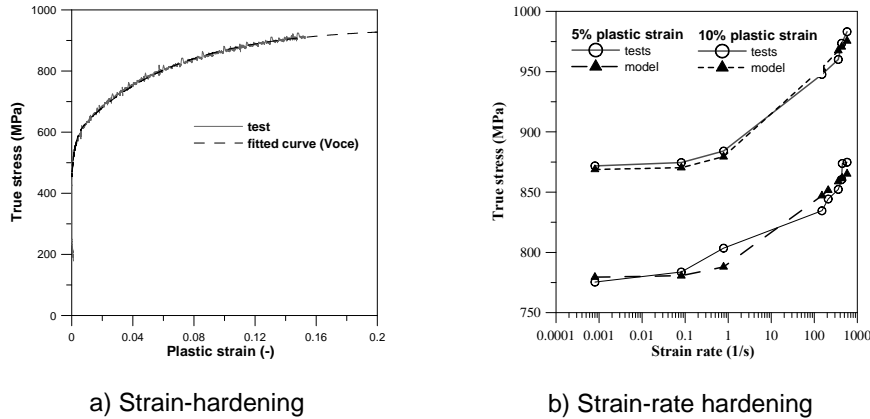


Figure 7. Comparison of test curves and fitted curve by Eq. (1).

In order to determine the strain-rate dependence, it is necessary to know the relation between the strain rate, $\dot{\bar{\epsilon}}$, and the effective stress, $\bar{\sigma}$, at a particular level of the plastic strain, $\bar{\epsilon}$. The flow stresses with respect to the strain-rates are displayed in Figure 7b, plotted on a semi-log scale at 5 % and 10 % plastic strain levels. The viscoplastic parameters were found by using least squares fit between the model represented by Eq. **Error! Reference source not found.** and the experimental data. The identified model is in good agreement with the experimental behaviour when $q = 0.0175$ and $\dot{\bar{\epsilon}}_0 = 0.78$ /s at a plastic strain of 10%, and the same model parameters also give good correspondence with the experimental behaviour at a plastic strain of 5 %, see Figure 7b.

4.2 Isotropic and Kinematic hardening parameters

Several procedures were exploited to obtain the individual components of isotropic and kinematic hardening from the simple uniaxial tests. It was chosen to separate the respective isotropic and kinematic components by introducing the following constraints

$$Q_{Xi} = \eta_i Q_i; \quad C_{Xi} = C_i, \quad (2)$$

$$Q_{Ri} = (1 - \eta_i) Q_i; \quad C_{Ri} = C_i \quad (3)$$

where the two fitting parameters η_1 and η_2 represents the percentage kinematic hardening of the two exponential terms. These parameters were deduced by numerical testing and correlation with the experimental Cauchy stress vs. logarithmic plastic strain curve for the specimen mts049002, which is chosen as the reference curve, reloaded in 90° direction after 4 % pre-straining. An extensive parametric study was accomplished to identify the parameters η_1 and η_2 to represent the trends of the experimental data. Simulations have been carried out by introducing various combinations for η_1 and η_2 from 0 to 1. The model and procedure have given reasonable results compared to the experimental data when the parameters are approximately $\eta_1 = 0.96$ and $\eta_2 = 0.47$, and the corresponding material parameters are given in **Error! Reference source not found.**, which are used to predict the response of the material behaviour under strain-path changes.

E	ν	Y_0	Q_{R1}	C_{R1}	Q_{R2}	C_{R2}	Q_{X1}	C_{X1}	Q_{X2}	C_{X2}
[GPa]	[-]	[MPa]	[MPa]	[-]	[MPa]	[-]	[MPa]	[-]	[MPa]	[-]
205	0.3	420	7.3	337	204	15	171	337	184	15

Table 2. Identified material parameters for DP800 from the experiments.

5 Numerical analyses

The experimental results of the tensile tests and shear tests with and without path changes are compared with analogous numerical results obtained with LS-DYNA. Figure 8 presents the numerical results of dynamic tensile tests and shear tests for the virgin material, DP800, obtained with isotropic hardening. Numerical simulations predicted very well the observed experimental responses.

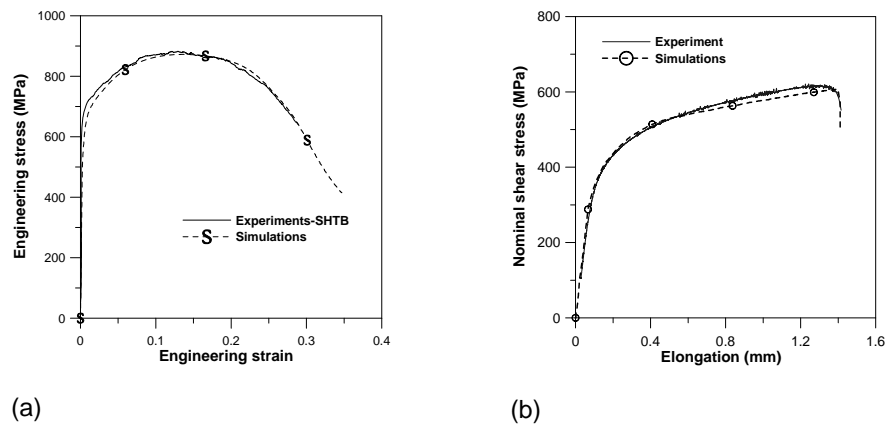


Figure 8. Comparison of experimental and numerical responses of (a) dynamic tensile test at 445 s^{-1} , and (b) Shear test.

Figure 9 shows uniaxial stress-strain curves at orientations 0° , 45° and 90° with respect to the rolling direction for the as-received sheet and for the 4 % pre-strained (tensile) sheets. The numerical simulations predict accurately the responses of the as-received material, as shown in Figure 9a. The general trends of the material behaviour after pre-straining are also captured fairly well by the numerical analyses albeit the work-hardening rate after the transient stage under strain-path changes is over-estimated for 4 % pre-strained sheet, see Figure 9b. Detailed information about the modelling of strain path changes in dual-phase steels are given in Tarigopula et al. [10, 11]. The same model was validated for crashworthiness of dual-phase high-strength steel sections [12].

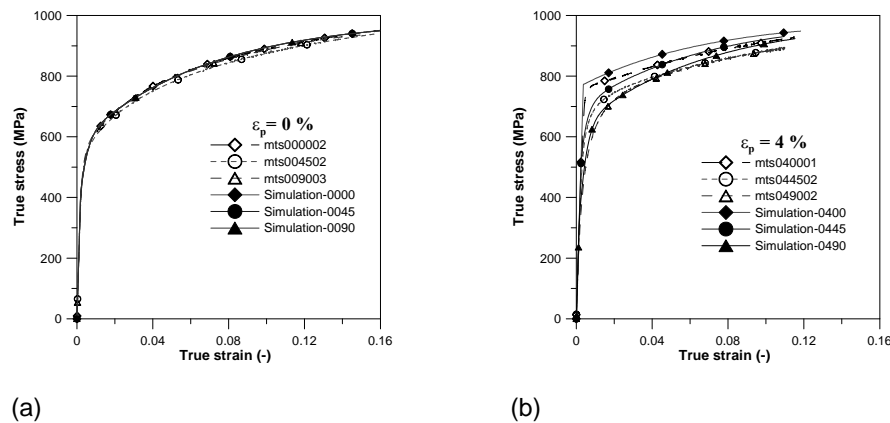


Figure 9. Comparison of experimental and numerical true stress-strain curves from tension tests of (a) as-received sheet and (b) 4 % pre-strained sheet in tension.

6 Conclusions

The combined isotropic and kinematic hardening model adopted in this study is able to represent the mechanical behaviour of dual-phase steels under various loading conditions.

7 Literature

- [1] Chaboche, J.L.: "Int. J. Plasticity", 2, 1986, 149-164.
- [2] Lemaitre, J. and Chaboche, J.L.: *Mechanics of Solid Materials*, "Cambridge University Press", 1990, 161-241.
- [3] Berstad, T., Lademo, O.-G. and Hopperstad, O.S.: *Weak and strong texture models in LS-DYNA (WTM-2D/3D and STM-2D)* "SINTEF Materials and Chemistry", SINTEF Report STF80MK F05180, 2005, Trondheim.
- [4] Clausen, A.H. and Auestad, T.: *Split-Hopkinson tension bar: Experimental set-up and theoretical considerations*, "SIMLab, Norwegian University of Science and Technology", Technical report R-16-02, 2002, Trondheim.
- [5] Lademo, O.-G., Eriksson, M., Reyes, A., Hopperstad, O.S. and Langseth, M.: *Characterisation of failure and identification of failure related parameters*, "SINTEF", Report No. STF80MK F06083, 2006, Trondheim.
- [6] Eriksson, M., Lademo, O.-G. and Hopperstad, O.S.: In: The 9th International ESAFORM conference on material forming, "Proceedings of ESAFORM 2006", April 26-28 2006, Glasgow.
- [7] Tarigopula, V. Hopperstad, O.S., Langseth, M., Clausen A.H., Hild, F., Lademo, O.-G. and Eriksson, M.: "Exp. Mech.", 48(2), 2008, 181-197.
- [8] Belytschko, T., Liu, W.K. and Moran, M.: *Nonlinear Finite Elements for Continua and Structures*, "Wiley", 2000.
- [9] Johnson, G.R. and Cook, W.H.: "In: Proceedings of Seventh International Symposium on Ballistics", The Hage.
- [20] Tarigopula, V., Hopperstad, O.S., Langseth, M. and Clausen, A.H.: "Eur. J. Mech-A/Solids", 27(5), 2008, 764-782.
- [31] Tarigopula, V., Hopperstad, O.S., Langseth, M. and Clausen, A.H.: "Eur. J. Mech-A/Solids", In Press, 2009.
- [42] Tarigopula, V., Langseth, M., Hopperstad, O.S. and Clausen, A.H.: "Int. J. Impact Engg.", 32(5), 2006, 847-882.